Available online at www.sciencedirect.com
ScienceDirect
International Journal of Heat and Mass Transfer 50 (2007) 3390–3400
International Journal of HEAT and MASS TRANSFER
www.elsevier.com/locate/ijhmt

Generalized stability theory of vapor film in subcooled film boiling on a sphere

Hiroshi Honda [a,*], Osamu Makishi [b], Hikaru Yamashiro [c]

[a] Kyushu University, Kasuyamachi, Kasuyagun, Fukuoka 811-2307, Japan
[b] Department of Mechanical Systems Engineering, Okinawa National College of Technology, Nago, Okinawa 905-2192, Japan
[c] Institute for Materials Chemistry and Engineering, Kyushu University, Kasuga, Fukuoka 816-8580, Japan

Received 19 July 2006; received in revised form 4 December 2006
Available online 30 March 2007

Abstract

The previously proposed stability theory of vapor film in subcooled film boiling on a sphere was generalized to take account of interaction between base flow and perturbed components. A disturbance of standing wave type was assumed to be superimposed on the base flows of surrounding liquid and vapor film. For the surrounding liquid, the wave equation was applied to the whole region including the boundary layer and the energy equation was solved analytically by introducing a simplifying assumption. For the vapor film, the basic equations were solved by an integral method. By use of compatibility conditions at the liquid–vapor interface, the solutions for the surrounding liquid and the vapor film were combined to yield an algebraic relation among the vapor film thickness, the order of disturbance and the complex amplification factor of disturbance. The numerical solutions of critical vapor film thickness at which the real part of complex amplification factor was equal to zero were obtained for the disturbances of the zeroth, first and second orders. The numerical results indicated that the vapor film was most unstable for the disturbance of the zeroth order (i.e., uniform disturbance). The calculated value of the critical vapor film thickness for the uniform disturbance compared well with the average vapor film thickness at the minimum-heat-flux point obtained from the immersion cooling experiments of spheres in water at high liquid subcoolings.
© 2007 Elsevier Ltd. All rights reserved.

Keywords: Subcooled film boiling; Minimum-heat-flux point; Linear stability analysis; Sphere

1. Introduction

The collapse of vapor film and the onset of liquid–solid contact in film boiling, which leads to the generation of minimum-heat-flux (MHF) point of the boiling curve, have received considerable attention due to its importance in the nuclear reactor safety, thermal stability of superconducting magnet, rapid solidification processing of metals, vapor explosion, etc. Many experimental and theoretical studies have been conducted to clarify the mechanism of the onset of liquid–solid contact and the MHF-point condition. An extensive review of relevant literature has been given by Nishio [1]. Experimental results [2–5] have shown that the MHF-point does not necessarily correspond to the limit of liquid–solid contact but it depends on the time and space fraction of the liquid–solid contact. Thus the MHF-point varies with system parameters such as surface configuration, thermophysical properties of test liquid and test surface, wettability of the test surface, liquid subcooling and system pressure.

The previously proposed theories of the MHF-point condition are divided into two categories [1]. The first is the temperature-controlled hypothesis [6–8] in which the liquid–solid contact is assumed to occur when the wall temperature decreases below the thermodynamic superheat limit of liquid. The second is the heat-flux controlled hypothesis [9–13] in which the MHF-point is assumed to be controlled by the Taylor instability [14] of liquid–vapor interface. Honda et al. [15–17] carried out a series of rapid

* Corresponding author. Tel./fax: +81 92 938 0570.
E-mail address: hhonda@pb4.so-net.ne.jp (H. Honda).

0017-9310/$ - see front matter © 2007 Elsevier Ltd. All rights reserved.
doi:10.1016/j.ijheatmasstransfer.2007.01.043

Nomenclature

C	specific heat at constant pressure
c	speed of sound
d	sphere diameter
h_k	spherical Hankel function of kth order
h_{lg}	latent heat of vaporization
k	order of disturbance
P_k	Legendre function of first kind of kth order
P	pressure
q	heat flux
r	radial coordinate
s	complex amplification factor of disturbance
T	temperature
ΔT_{sat}	wall superheat
ΔT_{sub}	liquid subcooling
t	time
u	circumferential velocity
v	radial velocity
y	coordinate measured outward normal to sphere surface
y^*	coordinate measured outward normal to liquid–vapor interface
α	heat transfer coefficient
δ	vapor film thickness
δ_t	thermal boundary layer thickness
κ	thermal diffusivity
λ	thermal conductivity
μ	viscosity
ρ	density
σ	surface tension
σ_r	Stefan–Boltzmann constant
ϕ	angular coordinate

Subscripts

c	bulk liquid, convection
cr	critical value
ev	evaporation
i	liquid–vapor interface
l	liquid
MHF	minimum-heat-flux point
r	radiation
v	vapor, vapor film
s	saturation
w	wall
0	base flow

Superscripts

$'$	perturbed component
$\sim$	instant of liquid–solid contact

quenching experiments of thin horizontal wires using water, $CaCl_2$/water solution and ethanol as quenching liquids. The experiments were conducted for a forced convection condition in which a heated platinum wire was forced to fall at a constant speed into a bath of quenching liquid [15,16] and for a free convection condition in which a platinum wire fixed in a liquid bath was instantaneously heated to a high temperature and then it was quenched by the surrounding liquid [17]. For both cases the behavior of the MHF-point could not be explained by the foregoing theories.

Honda et al. [18] have developed a new stability theory of vapor film for free convection film boiling on a sphere. In this theory, a small disturbance of standing wave type was assumed to be superimposed on the base flows of surrounding liquid and vapor film. The compressibility of surrounding liquid and the perturbation of evaporation rate due to the disturbance were taken into account. However, the effect of interaction between base flow and perturbed components was neglected. By using the compatibility condition at the liquid–vapor interface, the solutions for the surrounding liquid and the vapor film were combined to yield an algebraic relation among the vapor film thickness, the order of disturbance and the complex amplification factor of disturbance. The numerical solution of the critical vapor film thickness below which the vapor film was unstable was obtained for the disturbances of the orders of 0–3. The critical vapor film thickness was larger for a smaller order of disturbance, indicating that the onset of instability was determined by the critical vapor film thickness for the disturbance of the zeroth order (i.e., uniform disturbance). Comparison of the critical vapor film thickness for a uniform disturbance with the average vapor film thickness at the MHF-point obtained from the quenching experiments of spheres in subcooled water by Dhir–Purohit [19], Nishio–Uemura [8] and Kikuchi et al. [20] showed a fairly good agreement at high liquid subcoolings.

The objective of the present paper is to develop a more generalized theory taking account of interaction between the base flow and perturbed components for free convection film boiling on a sphere. The calculated values of the critical vapor film thickness for a uniform disturbance are compared with available experimental data of the average vapor film thickness at the MHF-point [8,19,20]. Comparison is also made with the prediction of the previously proposed theory [18].

2. Theoretical analysis

Fig. 1 shows the physical model of film boiling on a sphere immersed in a subcooled liquid. The radial coordinate is r and the angular coordinate measured from the bottom of the sphere is ϕ. The coordinate y is measured outward normal to the sphere surface. The vapor film thickness δ and the thickness of liquid boundary layer surrounding the vapor film are assumed to be sufficiently

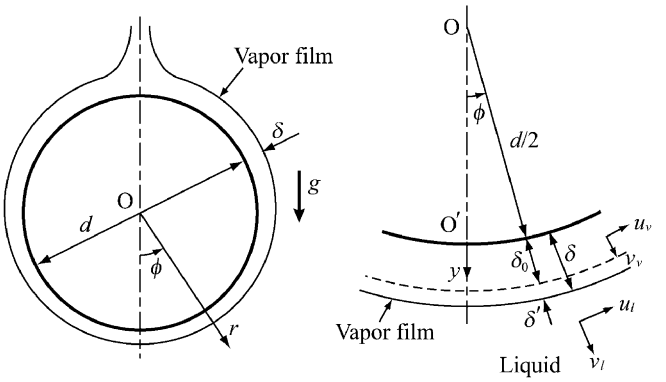

Fig. 1. Physical model and coordinates.

smaller than the sphere diameter d. The velocity components of surrounding liquid in the radial and circumferential directions are u_l and v_l, respectively, and those of vapor in the vapor film are u_v and v_v, respectively. A small disturbance of standing wave type which is symmetrical with respect to the vertical axis is assumed to be superimposed on the base flows of surrounding liquid and vapor film. The physical quantities of the base flow and the perturbed component are denoted by subscript $_0$ and superscript $'$, respectively. Thus $\delta = \delta_0 + \delta'$, $u_l = u_{l0} + u'_l$, etc. The subscript 0 is omitted for the physical properties.

2.1. Surrounding liquid

The surrounding liquid is divided into a boundary layer and a bulk liquid outside the boundary layer. When a small disturbance is superimposed, interaction occurs between the base flow and the perturbed component in the boundary layer. Such an interaction is negligible in the bulk liquid where liquid is almost stagnant. On the basis of the assumption that the boundary layer thickness is much smaller than the sphere diameter, it is assumed that the distribution of pressure disturbance in the liquid is determined by the solution of basic equations for the bulk liquid. The basic equations are

$$\frac{\partial \rho'_l}{\partial t} + \frac{1}{r^2}\frac{\partial}{\partial r}\left(\rho_l r v'_l\right) + \frac{1}{r\sin\phi}\frac{\partial}{\partial \phi}\left(\rho_l u'_l \sin\phi\right) = 0 \tag{1}$$

$$\rho_l \frac{\partial u'_l}{\partial t} + \frac{1}{r}\frac{\partial P'_l}{\partial \phi} = 0 \tag{2}$$

$$\rho_l \frac{\partial v'_l}{\partial t} + \frac{\partial P'_l}{\partial r} = 0 \tag{3}$$

where ρ_l is the liquid density, t is time and P'_l is the perturbed component of liquid pressure. Assuming an adiabatic change, ρ'_l and P'_l are related by the following equation:

$$P'_l = c_l^2 \rho'_l \tag{4}$$

where c_l is the speed of sound. Elimination of u'_l, v'_l and ρ'_l from Eqs. (1)–(4) yields the following equation:

$$\frac{1}{c_l^2}\frac{\partial^2 P'_l}{\partial t^2} = \frac{1}{r^2}\frac{\partial}{\partial r}\left(r^2\frac{\partial P'_l}{\partial r}\right) + \frac{1}{r^2\sin\phi}\frac{\partial}{\partial r}\left(\sin\phi\frac{\partial P'_l}{\partial \phi}\right) \tag{5}$$

Eq. (5) is called the wave equation. The boundary conditions are

$$P'_l = 0 \quad \text{at } r \to \infty \tag{6}$$

$$\partial P'_l/\partial\phi = 0 \quad \text{at } \phi = 0, \pi \tag{7}$$

The solution of Eq. (5) subject to the boundary conditions (6) and (7) is

$$P'_l = A_k h_k(\mathrm{i}sr/c_l)P_k(\cos\phi)\mathrm{e}^{st}, \quad k = 0, 1, 2\ldots \tag{8}$$

where h_k is the spherical Hankel function of the kth order, P_k is the Legendre function of the first kind of the kth order, $s = s_r + \mathrm{i}s_i$, s_r is the amplification factor of disturbance and s_i is the frequency of disturbance.

At the liquid–vapor interface, v'_l and δ' are related by the following equation:

$$v'_l = \frac{\partial \delta'}{\partial t} \quad \text{at } r = r_i = \frac{d}{2} + \delta \tag{9}$$

Substitution of p'_l and v'_l given by Eqs. (8) and (9) into Eq. (3) yields a differential equation for δ'. The solution of the resulting equation is

$$\delta' = \frac{A_k}{\rho_l c_l s}\left[\frac{(k+1)c_l}{sr_i}h_k\left(\mathrm{i}\frac{sr_i}{c_l}\right) - \mathrm{i}h_{k-1}\left(\mathrm{i}\frac{sr_i}{c_l}\right)\right]P_k(\cos\phi)\mathrm{e}^{st}, \quad k = 0, 1, 2\ldots \tag{10}$$

where h_{-1} is defined as

$$h_{-1}\left(\mathrm{i}\frac{sr_i}{c_l}\right) = -\frac{\mathrm{i}c_l}{sr_i}\exp\left(-\frac{sr_i}{c_l}\right) \tag{11}$$

In the case of $c_l/|s|r_i \gg 1$, Eq. (10) can be simplified as

$$\delta' = \frac{(k+1)A_k}{\rho_l r_i s^2}h_k\left(\mathrm{i}\frac{sr_i}{c_l}\right)P_k(\cos\phi)\mathrm{e}^{st} \tag{12}$$

According to the numerical results described in the next section, $2c_l/s_i d$ is of the order of 10^2. Thus Eq. (12) is satisfactory for the first approximation.

The liquid boundary layer oscillates as the liquid–vapor interface oscillates. Taking the coordinate y^* outward normal to the liquid–vapor interface, the energy equation for the perturbed component is written as

$$\frac{\partial T'_l}{\partial t} + \frac{2u'_l}{d}\frac{\partial T_{l0}}{\partial \phi} + \frac{2u_{l0}}{d}\frac{\partial T'_l}{\partial \phi} + v'_l\frac{\partial T_{l0}}{\partial y^*} + v_{l0}\frac{\partial T'_l}{\partial y^*} = \kappa_l\frac{\partial^2 T'_l}{\partial y^{*2}} \tag{13}$$

where T_{l0} is the liquid temperature of the base flow, T'_l is the perturbed component of liquid temperature and κ_l is the thermal diffusivity of liquid. Neglecting the ϕ-component and introducing the simplifying assumptions $v'_l = q'_{ev}/\rho_l h_{lg}$ and $v_{l0} = q_{ev0}/\rho_l h_{lg}$, Eq. (13) is simplified as

$$\frac{\partial T'_l}{\partial t} - \frac{q'_{ev}}{\rho_l h_{lg}}\frac{\partial T_{l0}}{\partial y^*} - \frac{q_{ev0}}{\rho_l h_{lg}}\frac{\partial T'_l}{\partial y^*} = \kappa_l\frac{\partial^2 T'_l}{\partial y^{*2}} \tag{14}$$

where $q'_{ev} = q'_\delta - q'_c$ is the perturbed component of evaporating heat flux, $q'_\delta = -\lambda_v(\partial T'_v/\partial y)_\delta$, $q'_c = -\lambda_l(\partial T'_l/\partial y^*)_0$,

$q_{ev0} = \lambda_v \Delta T_{sat}/\delta_0 + \alpha_r \Delta T_{sat} - \alpha_c \Delta T_{sub}$ is the evaporating heat flux of the base flow, λ_l is the thermal conductivity of liquid, λ_v is the thermal conductivity of vapor, h_{lg} is the latent heat of evaporation, $\alpha_r = \sigma_r(T_w^4 - T_s^4)/\Delta T_{sat}$ is the heat transfer coefficient of radiation, α_c is the convection heat transfer coefficient, σ_r is the Stefan–Boltzmann constant, $\Delta T_{sat} = T_w - T_s$ is the wall superheat, $\Delta T_{sub} = T_s - T_c$ is the liquid subcooling, T'_v is the perturbed component of vapor temperature, T_w is the wall temperature, T_s is the saturation temperature and T_c is the bulk liquid temperature. The distribution of T_{l0} is assumed as

$$T_{l0} = \Delta T_{sub} \exp\left(-\frac{y^*}{\delta_t}\right) + T_c \tag{15}$$

where $\delta_t = \lambda_l/\alpha_c$ is the thermal boundary layer thickness. The boundary conditions are

$$T'_l = T'_\delta = (dT_s/dP_s)P'_v \quad \text{at } y^* = 0 \tag{16}$$

$$T'_l = 0 \quad \text{at } y^* = \infty \tag{17}$$

where dT_s/dP_s is the slope of the saturation temperature curve. The solution of Eq. (14) subject to the boundary conditions (16) and (17) is

$$T'_l = T'_\delta \exp\left[-\frac{1}{2}\left(a_1 + \sqrt{a_1^2 + a_2}\right)y^*\right] - \frac{q'_{ev}\Delta T_{sub}}{\rho_l h_{lg}\delta_t(s - \kappa_l/\delta_t^2 + q_{ev0}/\rho_l h_{lg}\delta_t)} \exp\left(-\frac{y^*}{\delta_t}\right) \tag{18}$$

where $a_1 = q_{ev0}/\kappa_l\rho_l h_{lg}$ and $a_2 = s/\kappa_l$. In the case of $\sqrt{a_2} \gg a_1$ and $s \gg (\kappa_l/\delta_t^2 - q_{ev0}/\rho_l h_{lg}\delta_t)$, Eq. (18) can be simplified as

$$T'_l = T'_\delta \exp\left\{-\left(\frac{\lambda_l q_{v0}}{2\kappa_l\rho_l h_{lg}} + \lambda_l\sqrt{\frac{s}{\kappa_l}}\right)y^*\right\} - \frac{\alpha_c \Delta T_{sub} q'_{ev}}{\rho_l\lambda_l h_{lg} s} \exp\left(-\frac{y^*}{\delta_t}\right) \tag{19}$$

According to the numerical results, $\sqrt{a_2}/a_1$ and $s/(\kappa_l/\delta_t^2 - q_{ev0}/\rho_l h_{lg}\delta_t)$ are of the order of 10^3 and 10^2, respectively. Thus Eq. (19) is accurate enough for the first approximation. Substitution of Eq. (19) into the definition of q'_c yields the following solution:

$$q'_c = \left(\frac{\lambda_l q_{v0}}{2\kappa_l\rho_l h_{lg}} + \lambda_l\sqrt{\frac{s}{\kappa_l}}\right)T'_\delta - \frac{\alpha_c^2 \Delta T_{sub} q'_{ev}}{\rho_l h_{lg}\lambda_l s} \tag{20}$$

2.2. Vapor film

Integration of the equations of continuity, momentum and energy for the perturbed component across the vapor film thickness yields the following equations:

$$\frac{\partial \rho'_v}{\partial t}\delta_0 + \frac{2}{d}\frac{\partial \rho'_v}{\partial \phi}\int_0^{\delta_0} u_{v0}\,dy + \frac{2}{d}\cot\phi\left(\rho'_v\int_0^{\delta_0} u_{v0}\,dy + \rho_v\int_0^{\delta} u'_v\,dy\right) + \frac{2}{d}\left(\rho'_v\int_0^{\delta_0}\frac{\partial u_{v0}}{\partial\phi}\,dy + \rho_v\int_0^{\delta}\frac{\partial u'_v}{\partial\phi}\,dy\right) + \rho_v\left(\frac{\partial\delta'}{\partial t} - \frac{q'_{ev}}{\rho_v h_{lg}}\right) = 0 \tag{21}$$

$$\rho_v\int_0^{\delta}\frac{\partial u'_v}{\partial t}\,dy + \frac{2}{d}\int_0^{\delta}\left(u_{v0}\frac{\partial u'_v}{\partial\phi} + u'_v\frac{\partial u_{v0}}{\partial\phi}\right)dy + \int_0^{\delta}\left(v_{v0}\frac{\partial u'_v}{\partial y} + v'_v\frac{\partial u_{v0}}{\partial y}\right)dy = (\rho_l - \rho_v)g\sin\phi\,\delta' - \frac{2}{d}\frac{\partial P'_v}{\partial\phi}\delta + \mu_v\left\{\left(\frac{\partial u_v}{\partial y}\right)_0^{\delta} - \left(\frac{\partial u_{v0}}{\partial y}\right)_0^{\delta_0}\right\} \tag{22}$$

$$\int_0^{\delta}\frac{\partial T'_v}{\partial t}\,dy + \frac{2}{d}\int_0^{\delta}\left(u_{v0}\frac{\partial T'_v}{\partial\phi} + u'_v\frac{\partial T_{v0}}{\partial\phi}\right)dy + \int_0^{\delta}\left(v_{v0}\frac{\partial T'_v}{\partial y} + v'_v\frac{\partial T_{v0}}{\partial y}\right)dy = \kappa_v\left\{\left(\frac{\partial T_v}{\partial y}\right)_0^{\delta} - \left(\frac{\partial T_{v0}}{\partial y}\right)_0^{\delta_0}\right\} \tag{23}$$

where

$$\rho'_v = \frac{\rho_v}{P_{v0}}\left(1 - \frac{P_{v0}}{2T_m}\frac{dT_s}{dP_s}\right)P'_v \tag{24}$$

$$P'_v = P'_{li} - \frac{4\sigma}{d^2}\left(\frac{\partial^2\delta'}{\partial\phi^2} + \cot\phi\frac{\partial\delta'}{\partial\phi}\right) - \frac{8\sigma\delta'}{d^2} \tag{25}$$

$$u_{v0} = -\frac{(\rho_l - \rho_v)g\sin\phi}{2\mu_v}(by^2 - \delta_0 y), \quad 0.5 < b < 1 \tag{26}$$

$$T_{v0} = T_w - \Delta T_{sat}\frac{y}{\delta_0} \tag{27}$$

ρ_v is the vapor density, ρ'_v is the perturbed component of vapor density, g is the gravitational acceleration, κ_v is the thermal diffusivity of vapor, μ_v is the vapor viscosity, σ is the surface tension, P'_v is the perturbed component of vapor pressure, P_{v0} is the vapor pressure of the base flow , P'_{li} is the perturbed component of liquid pressure at the liquid–vapor interface, and $T_m = (T_w + T_s)/2$. The surface tension terms in Eq. (25) are obtained from the geometrical relation of the vapor film. Since $\delta \ll d$, substitution of $r_i = d/2 + \delta \approx d/2$ into Eq. (8) yields the following approximate solution for P'_{li}:

$$p'_{li} = A_k h_k(isd/2c_l)P_k(\cos\phi)e^{st} \tag{28}$$

Neglecting the surface tension terms in Eq. (25), we obtain

$$P'_v = P'_{li} = A_k h_k(isd/2c_l)P_k(\cos\phi)e^{st} \tag{29}$$

According to the numerical results, the ratio of the surface tension terms in Eq. (25) to P'_{li} is of the order of 10^{-6}. Thus Eq. (29) is accurate enough for the present analysis. The

value of b in Eq. (26) is determined by solving the basic equations for the base flow. Numerical solutions of film boiling on a vertical surface by Koh [21] suggest that b is close to unity for conventional fluids at the atmospheric pressure.

If the absolute value of s is sufficiently large, the space derivative terms on the left-hand-side of Eqs. (22) and (23) are negligible as compared to the time derivative term. Thus Eqs. (22) and (23) can be simplified as follows:

$$\rho_v \int_0^\delta \frac{\partial u'_v}{\partial t}\,dy = (\rho_l-\rho_v)g\sin\phi\,\delta' - \frac{2}{d}\frac{\partial P'_v}{\partial \phi}\delta + \mu_v\left\{\left(\frac{\partial u_v}{\partial y}\right)_0^{\delta} - \left(\frac{\partial u_{v0}}{\partial y}\right)_0^{\delta_0}\right\} \tag{30}$$

$$\int_0^\delta \frac{\partial T'_v}{\partial t}\,dy = \kappa_v\left\{\left(\frac{\partial T_v}{\partial y}\right)_0^{\delta} - \left(\frac{\partial T_{v0}}{\partial y}\right)_0^{\delta_0}\right\} \tag{31}$$

According to the numerical results, the ratio of the space derivative terms to the time derivative term in Eqs. (22) and (23) is of the order of 10^{-2}. Thus Eqs. (30) and (31) are accurate enough for the first approximation.

Taking account of the boundary conditions at the wall and at the liquid–vapor interface, the distributions of u_v and T_v are assumed as

$$u_v = -\frac{(\rho_l-\rho_v)g\sin\phi}{2\mu_v}(by^2-\delta y) + f_1(\phi)e^{st}(y^2-\delta y) \tag{32}$$

$$T_v = T_w - (\Delta T_{sat} - T'_\delta)\frac{y}{\delta} + f_2(\phi)e^{st}(y^2-\delta y) \tag{33}$$

Substitution of Eqs. (32) and (33) into Eqs. (30) and (31), respectively, yields the following solutions for f_1 and f_2:

$$f_1 e^{st} = \left\{\frac{1}{\mu_v d}\frac{\partial P'_v}{\partial\phi} + \frac{\rho_v(\rho_l-\rho_v)g\sin\phi}{8\mu_v^2}\delta\frac{\partial\delta'}{\partial t} + \frac{(b-1)(\rho_l-\rho_v)g\sin\phi}{2\mu_v\delta}\delta'\right\}\left(1+\frac{\rho_v s\delta^2}{12\mu_v}\right)^{-1} \tag{34}$$

$$f_2 e^{st} = \left(\frac{\Delta T_{sat}}{4\kappa_v}\frac{1}{\delta}\frac{\partial\delta'}{\partial t} + \frac{1}{4\kappa_v}\frac{\partial T'_\delta}{\partial t}\right)\left(1+\frac{s\delta^2}{12\kappa_v}\right)^{-1} \tag{35}$$

In the case of $\rho_v s\delta^2/12\mu_v \ll 1$ and $s\delta^2/12\kappa_v \ll 1$, Eqs. (34) and (35) can be simplified as

$$f_1 e^{st} = \frac{1}{\mu_v d}\frac{\partial P'_v}{\partial\phi} + \frac{\rho_v(\rho_l-\rho_v)g\sin\phi}{8\mu_v^2}\delta\frac{\partial\delta'}{\partial t} + \frac{(b-1)(\rho_l-\rho_v)g\sin\phi}{2\mu_v\delta}\delta' \tag{36}$$

$$f_2 e^{st} = \left(\frac{\Delta T_{sat}}{4\kappa_v}\frac{1}{\delta}\frac{\partial\delta'}{\partial t} + \frac{1}{4\kappa_v}\frac{\partial T'_\delta}{\partial t}\right) \tag{37}$$

According to the numerical results, $\rho_v s\delta^2/12\mu_v$ and $s\delta^2/12\kappa_v$ are of the order of 10^{-3} to 10^{-2}. Thus Eqs. (36) and (37) are accurate enough for the first approximation. Substitution of Eqs. (36) and (37) into Eqs. (32) and (33), respectively, yields the following solutions for u'_v and T'_v:

$$u'_v = u_v - u_{v0} = \frac{(\rho_l-\rho_v)g\sin\phi}{2\mu_v}\delta' y + \left\{\frac{1}{\mu_v d}\frac{\partial P'_v}{\partial\phi} + \frac{\rho_v(\rho_l-\rho_v)g\sin\phi}{8\mu_v^2}\delta_0\frac{\partial\delta'}{\partial t} + \frac{(b-1)(\rho_l-\rho_v)g\sin\phi}{2\mu_v\delta}\delta'\right\}(y^2-\delta y) \tag{38}$$

$$T'_v = T_v - T_{v0} = \left(\frac{\Delta T_{sat}}{\delta_0^2}\delta' + \frac{T'_\delta}{\delta_0}\right)y + \left(\frac{\Delta T_{sat}}{4\kappa_v}\frac{1}{\delta_0}\frac{\partial\delta'}{\partial t} + \frac{1}{4\kappa_v}\frac{\partial T'_\delta}{\partial t}\right)(y^2-\delta y) \tag{39}$$

Substitution of T'_l and T'_v given by Eqs. (19) and (39), respectively, into the definition of q'_{ev} yields the following solution:

$$q'_{ev} = -\left\{\lambda_v\left(\frac{\Delta T_{sat}}{\delta_0^2}\delta' + \frac{T'_\delta}{\delta_0} + \frac{\Delta T_{sat}}{4\kappa_v}\frac{\partial\delta'}{\partial t} + \frac{\delta_0}{4\kappa_v}\frac{\partial T'_\delta}{\partial t}\right) + \left(\frac{\lambda_l q_{ev0}}{2\kappa_l\rho_l h_{lg}} + \lambda_l\sqrt{\frac{s}{\kappa_l}}\right)T'_\delta\right\}\left[1-\frac{\alpha_c^2\Delta T_{sub}}{\rho_l\lambda_l h_{lg}s}\right]^{-1} \tag{40}$$

In the case of $\alpha_c^2\Delta T_{sub}/\rho_l\lambda_l h_{lg}|s| \ll 1$, Eq. (40) can be simplified as

$$q'_{ev} = -\lambda_v\left(\frac{\Delta T_{sat}}{\delta_0^2}\delta' + \frac{T'_\delta}{\delta_0} + \frac{\Delta T_{sat}}{4\kappa_v}\frac{\partial\delta'}{\partial t} + \frac{\delta_0}{4\kappa_v}\frac{\partial T'_\delta}{\partial t}\right) - \left(\frac{\lambda_l q_{ev0}}{2\kappa_l\rho_l h_{lg}} + \lambda_l\sqrt{\frac{s}{\kappa_l}}\right)T'_\delta \tag{41}$$

According to the numerical results, $\alpha_c^2\Delta T_{sub}/\rho_l\lambda_l h_{lg}s_i$ is of the order of 10^{-5} to 10^{-4}. Thus Eq. (41) is accurate enough for the present analysis.

Substitution of u'_v and q'_{ev} given by Eqs. (38) and (41), respectively, into Eq. (21) yields the following equation:

$$\begin{aligned}&\frac{\partial\rho'_v}{\partial t}\delta_0 + \rho_v\frac{\partial\delta'}{\partial t} + \frac{(3-2b)(\rho_v-\rho_l)g\sin\phi}{6\mu_v d}\delta_0^3\frac{\partial\rho'_v}{\partial\phi} - \frac{\rho_v}{3\mu_v d^2}\left(\frac{\partial^2 P'_v}{\partial\phi^2} + \cot\phi\frac{\partial P'_v}{\partial\phi}\right)\delta_0^3 + \frac{(4-b)\rho_v(\rho_l-\rho_v)g\cos\phi}{3\mu_v d}\delta_0^2\delta' \\ &+ \frac{(\rho_l-\rho_v)g}{2\mu_v d}\left[\frac{(3-2b)\cos\phi}{3}\delta_0^3 + \sin\phi\frac{\partial\delta}{\partial\phi}\delta_0^2\right]\rho'_v + \frac{\rho_v(\rho_l-\rho_v)g\sin\phi}{2\mu_v d}\delta_0^2\frac{\partial\delta'}{\partial\phi} - \frac{\rho_v}{\mu_v d^2}\frac{\partial\delta_0}{\partial\phi}\frac{\partial P'_v}{\partial\phi}\delta_0^2 \\ &- \frac{\rho_v^2(\rho_l-\rho_v)g}{24\mu_v^2 d}\left(\cos\phi\delta_0^4\frac{\partial\delta'}{\partial t} + \sin\phi\delta_0^4\frac{\partial^2\delta'}{\partial\phi\partial t} + 4\sin\phi\delta_0^3\frac{\partial\delta_0}{\partial\phi}\frac{\partial\delta'}{\partial t}\right) \\ &+ \frac{\lambda_v}{h_{lg}}\left(\frac{\Delta T_{sat}}{\delta_0^2}\delta' + \frac{T'_\delta}{\delta_0} + \frac{\Delta T_{sat}}{4\kappa_v}\frac{\partial\delta'}{\partial t} + \frac{\delta_0}{4\kappa_v}\frac{\partial T'_\delta}{\partial t}\right) \\ &+ \frac{1}{h_{lg}}\left(\frac{\lambda_l q_{ev0}}{2\kappa_l\rho_l h_{lg}} + \lambda_l\sqrt{\frac{s}{\kappa_l}}\right)T'_\delta = 0\end{aligned} \tag{42}$$

Substitution of the solutions of P'_v, δ', ρ'_v and T'_δ given by Eqs. (29), (12), (24) and (16), respectively, into Eq. (42) yields an algebraic relation among δ_0, s and k. Then, substitution of $s = is_i$ (i.e., $s_r = 0$) into the resulting equation

yields an algebraic relation among the critical vapor film thickness below which the vapor film is unstable δ_{cr}, s_i and k.

In the present paper, the solution of s as a function of δ_0 is obtained for the combinations of $\phi = 0$ and $k = 0, 1$ and 2. Assuming $b = 1$ in Eq. (42), the equation to be solved is written as

$$\begin{aligned}&\left\{\frac{\delta_0}{P_{v0}}\left(1-\frac{P_{v0}}{2T_m}\frac{dT_s}{dP_s}\right)+\frac{C_v\delta_0}{4h_{lg}}\frac{dT_s}{dP_s}\right\}s^3\\&+\left\{\frac{k(k+1)\delta_0^3}{3\mu_v d^2}+\frac{(\rho_l-\rho_v)g\delta_0^3}{6\mu_v dP_v}\left(1-\frac{P_{v0}}{2T_m}\frac{dT_s}{dP_s}\right)\right.\\&\left.+\left(\frac{\lambda_v}{\rho_v h_{lg}\delta_0}+\frac{C_1 q_{ev0}}{2\rho_v h_{lg}^2}+\frac{\lambda_l}{\rho_v h_{lg}}\sqrt{\frac{s}{\kappa_l}}\right)\frac{dT_s}{dP_s}\right\}s^2\\&+(k+1)\left\{\frac{2}{\rho_l d}+\frac{C_v\Delta T_{sat}}{2h_{lg}\rho_l d}-\frac{\rho_v(\rho_l-\rho_v)g\delta_0^4}{12\mu_v^2\rho_l d^2}\right\}s\\&+2(k+1)\left\{\frac{\lambda_v\Delta T_{sat}}{\rho_l\rho_v h_{lg}d\delta_0^2}+\frac{(\rho_l-\rho_v)g\delta_0^2}{\rho_l\mu_v d^2}\right\}=0\end{aligned}\tag{43}$$

The solution of δ_{cr} and the corresponding value of s_i are obtained for the combinations of $\phi = 0$ and $k = 0, 1$ and 2, and for $\phi = \pi/2$ and $k = 0$. The equation to be solved is

$$\begin{aligned}&-\left\{\frac{\delta_{cr}}{P_{v0}}\left(1-\frac{P_{v0}}{2T_m}\frac{dT_s}{dP_s}\right)+\frac{C_v\delta_{cr}}{4h_{lg}}\frac{dT_s}{dP_s}\right\}is_i^3\\&-\left[\frac{k(k+1)\delta_{cr}^3}{3\mu_v d^2}+\frac{(\rho_l-\rho_v)g\delta_{cr}^3}{6\mu_v dP_v}\left(1-\frac{P_{v0}}{2T_m}\frac{dT_s}{dP_s}\right)\right.\\&\left.+\left\{\frac{\lambda_v}{\rho_v h_{lg}\delta_{cr}}+\frac{C_1 q_{evo}}{2\rho_v h_{lg}^2}+\frac{\lambda_l}{\rho_v h_{lg}}\sqrt{\frac{s_i}{2\kappa_l}}(1+i)\frac{dT_s}{dP_s}\right\}\right]s_i^2\\&+(k+1)\left\{\frac{2}{\rho_l d}+\frac{C_v\Delta T_{sat}}{2h_{lg}\rho_l d}-\frac{\rho_v(\rho_l-\rho_v)g\delta_{cr}^4}{12\mu_v^2\rho_l d^2}\right\}is_i\\&+2(k+1)\left\{\frac{\lambda_v\Delta T_{sat}}{\rho_l\rho_v h_{lg}d\delta_{cr}^2}+\frac{(\rho_l-\rho_v)g\delta_{cr}^2}{\rho_l\mu_v d^2}\right\}=0\end{aligned}\tag{44}$$

for $\phi = 0$ where $T_m = T_w + T_s/2$, and

$$\begin{aligned}&-\left\{\frac{\delta_{cr}}{P_{v0}}\left(1-\frac{P_{v0}}{2T_m}\frac{dT_s}{dP_s}\right)+\frac{C_v\delta_{cr}}{4h_{lg}}\frac{dT_s}{dP_s}\right\}is_i^3\\&-\left[\frac{(\rho_l-\rho_v)g\delta_{cr}^2}{2\mu_v dP_{v0}}\left(1-\frac{P_{v0}}{2T_m}\frac{dT_s}{dP_s}\right)\frac{\partial\delta_0}{\partial\phi}\right.\\&\left.+\left\{\frac{\lambda_v}{\rho_v h_{lg}\delta_{cr}}+\frac{C_1 q_{evo}}{2\rho_v h_{lg}^2}+\frac{\lambda_l}{\rho_v h_{lg}}\sqrt{\frac{s_i}{2\kappa_l}}(1+i)\right\}\frac{dT_s}{dP_s}\right]s_i^2\\&+\left\{\frac{2}{\rho_l d}+\frac{C_v\Delta T_{sat}}{2\rho_l h_{lg}d}-\frac{(k+1)\rho_v(\rho_l-\rho_v)g}{3\mu_v\rho_l d^2}\delta_{cr}^3\frac{\partial\delta_0}{\partial\phi}\right\}is_i\\&+\frac{2(\rho_l-\rho_v)g\delta_{cr}^2}{\rho_l\mu_v d^2}+\frac{2\lambda_v\Delta T_{sat}}{\rho_l\rho_v h_{lg}d\delta_{cr}^2}=0\end{aligned}\tag{45}$$

for $\phi = \pi/2$ and $k = 0$. The value of q_{ev0} in Eqs. (43)–(45) is obtained from its defining equation if α_c is known. However, the expression for α_c is not available. Thus, q_{ev0} was estimated by using the following equation which was obtained from the relation between the heat transfer rate and the flow rate of vapor leaving the sphere (see Appendix):

$$q_{ev0} = (\alpha_{vs} + 0.88\alpha_r)\left(\frac{\alpha_{vs}\delta_0}{\lambda_v}\right)^3\Delta T_{sat}\tag{46}$$

where α_{vs} is the heat transfer coefficient for saturated film boiling without radiation and $0.88\alpha_r$ is the correction term for the radiation effect proposed by Nishio–Uemura [8]. The value of α_{vs} was estimated by using an equation proposed by Kikuchi et al. [20] which was obtained from an approximate theoretical analysis of base flow assuming a parabolic distribution of velocity and a linear distribution of temperature in the vapor film and parabolic distributions of velocity and temperature in the liquid boundary layer. The value of $d\delta_0/d\phi$ in Eq. (45) was obtained from an approximate numerical analysis of the base flow.

2.3. Comparison of numerical results with experiments

Numerical solutions were obtained for the conditions of immersion cooling experiments of spheres in subcooled water conducted by Nishio–Uemura [8], Dhir–Purohit [19] and Kikuchi et al. [20]. In the numerical calculation, the physical properties of vapor and liquid were evaluated at the mean temperatures of vapor film and liquid boundary layer, respectively. Table 1 shows a summary of the experimental conditions. In the experiments of Nishio–Uemura [8], the test sphere of 10 mm in diameter was soldered to the lower end of a vertical stem of 2 mm in diameter. In the experiments of Dhir–Purohit [19], the test spheres of 19 mm in diameter were mounted on a vertical stem of 3 mm in diameter. To avoid premature collapse of vapor film due to the propagation of receding film front along the stem, a collar of 6 mm in diameter was welded on the stem at a distance of 5 mm from the sphere. The test piece of Kikuchi et al. [20] consisted of a spherical part of 30 mm in diameter and a cylindrical part of 8 mm in diameter and 10 mm in height which was connected to the top of the spherical part. The cylindrical part was soldered to the lower end of a vertical stem of 4 mm in diameter and the test piece was immersed in a water bath up to the middle of the cylindrical part. Kikuchi et al. [20]

Table 1
Experimental conditions

Author	Material	Surface condition	Immersion depth	d, mm	ΔT_{sub}, K
Nishio–Uemura	Silver	Clean	$1.8d$	10	1–73
Dhir–Purohit	Stainless steel				10–50
	Copper	Clean	Not specified	19	10–30
	Silver				10–20
Kikuchi et al.	Silver	Clean	$\approx 1.2d$	30	20–85
		Paint coated			20–80

conducted experiments with both a clean sphere and a sphere coated with a silicone-based heat resistant paint. The thickness of coating ranged from 5 μm to 27 μm.

During the experiments, two types of collapse mode were observed for the vapor film depending on the experimental conditions. The first was an instantaneous collapse in which the vapor film on the sphere collapsed almost instantaneously. The second was a propagative collapse in which the vapor film started to collapse near the connecting point between the test sphere and the stem and then the collapse propagated all over the sphere. According to Nishio–Uemura [8], Dhir–Purohi [19] and Kikuchi et al. [20], the experimental data adopted in the present paper are those for the instantaneous collapse.

Fig. 2 shows the wall superheat at the MHF-point $\Delta T_{sat,MHF}$ plotted as a function of ΔT_{sub} for all data. In Fig. 2, the limiting liquid superheat for water predicted by the Lienhard [22] equation (= 217.3 K) and an empirical equation for $\Delta T_{sat,MHF}$ proposed by Dhir–Purohit [19] are also shown for comparison. For the experimental data by Dhir–Purohit [19], $\Delta T_{sat,MHF}$ increases sharply as ΔT_{sub} increases. The experimental data by Nishio–Uemura [8] show a gentle increase in the range of $\Delta T_{sub} \geqslant 30$ K. The experimental data for the clean sphere by Kikuchi et al. [20] show no dependence on ΔT_{sub}. The measured values of $\Delta T_{sat,MHF}$ are scattered in a range and they are smaller than the limiting liquid superheat except for one data point. The experimental data for the paint-coated sphere by Kikuchi et al. [20] also show no dependence on ΔT_{sub}. The values of $\Delta T_{sat,MHF}$ are much larger than those for the clean sphere and most of them are higher than the limiting liquid superheat. It is seen from Fig. 2 that $\Delta T_{sat,MHF}$ changes widely depending on the experimental conditions and it can not be correlated as a function of ΔT_{sub}.

Fig. 3a and b, respectively, shows the calculated values of s_r and s_i for $k = 0$, 1 and 2 for the conditions of $d = 10$ mm, $\Delta T_{sat} = 200$ K and $\Delta T_{sub} = 70$ K plotted as a function of δ_0. The s_r curves in Fig. 3a cross the horizontal axis ($s_r = 0$) only once. As described previously, the value

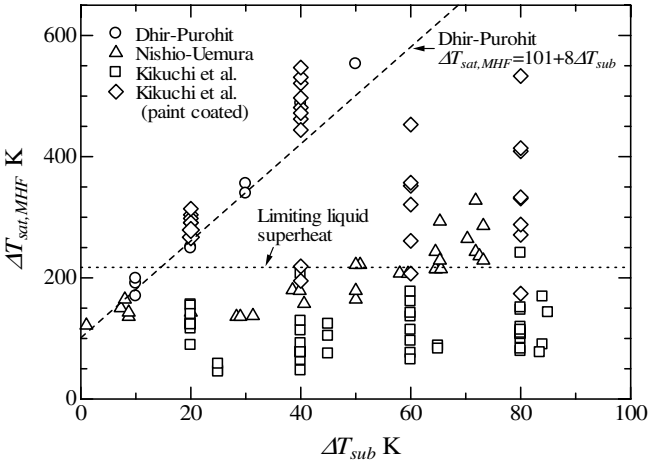

Fig. 2. Relation between ΔT_{sub} and $\Delta T_{sat,MHF}$.

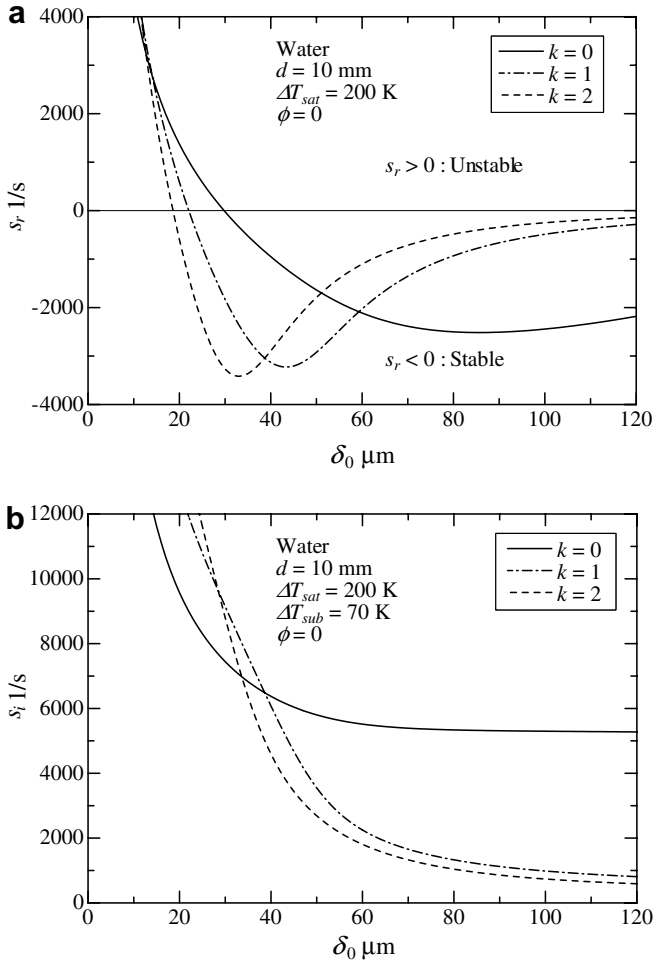

Fig. 3. Variation of s_r and s_i with δ_0.

of δ_0 at $s_r = 0$ is δ_{cr}. It is also seen from Fig. 3a that $s_r > 0$ for $\delta_0 < \delta_{cr}$ and $s_r < 0$ for $\delta_0 > \delta_{cr}$, which means that the vapor film is unstable for $\delta_0 < \delta_{cr}$ and vice versa. The value of δ_{cr} is larger for smaller k. Thus the stability of vapor film is determined by the largest value of δ_{cr} (= 29.8 μm) which corresponds to the disturbance of $k = 0$ (i.e., uniform disturbance). This value is denoted as δ_{cr0}. The values of s_i in Fig. 3b decrease monotonically as δ_0 increases. The value of s_i corresponding toδ_{cr0} is 7.47 kHz.

Fig. 4 shows the calculated values of δ_{cr} for the experimental conditions of Nishio–Uemura [8] plotted as a function of ΔT_{sat} with ϕ, k, and ΔT_{sub} as parameters.. The numerical results are presented for the set of conditions of $\phi = 0$, $k = 0$, 1 and 2, and $\Delta T_{sub} = 5$ K, 30 K, 58 K and 72 K, and for $\phi = \pi/2$ rad, $k = 0$ and $\Delta T_{sub} = 5$ K, 30 K, 58 K and 72 K. In Fig. 4, the values of δ_{cr} obtained from the theoretical model of Honda et al. [18] are also shown for comparison. Honda et al. [18] considered the pressure difference between liquid and vapor due to the surface tension effect but neglected the interaction between base flow and perturbed components. As described previously, the surface tension effect is negligible for practical

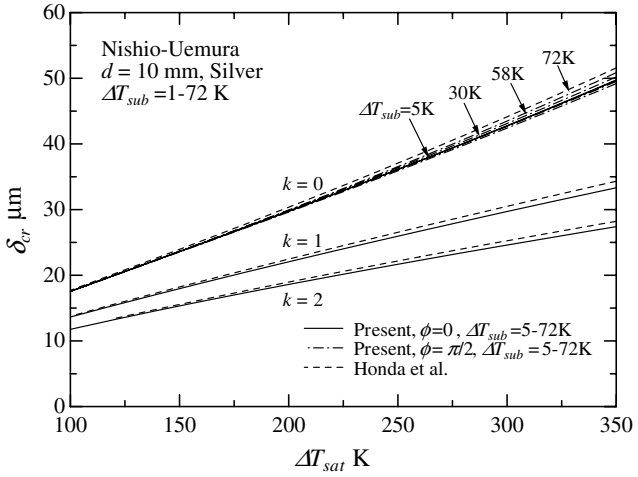

Fig. 4. Variation of δ_{cr} with ΔT_{sat}.

cases. Neglecting the surface tension terms, the equation corresponding to Eq. (42) is written as

$$\frac{\partial \rho'_v}{\partial t}\delta_0 + \rho_v \frac{\partial \delta'}{\partial t} - \frac{\rho_v}{3\mu_v d^2}\left(\frac{\partial^2 P'_v}{\partial \phi^2} + \cot\phi \frac{\partial P'_v}{\partial \phi}\right)\delta_0^3 + \frac{\lambda_v}{h_{lg}}\left(\frac{\Delta T_{sat}}{\delta_0^2}\delta' + \frac{T'_\delta}{\delta_0}\right) + \frac{\lambda_l}{h_{lg}}\sqrt{\frac{s}{\kappa_l}}T'_\delta = 0 \quad (47)$$

Since the effect of base flow is neglected in this theory, only one solution is obtained for each k. Comparison of the present and previous results reveals that the slope of the curve is slightly smaller for the present results. For each k, the two curves cross at $\Delta T_{sat} \approx 100$ K and the present solution is smaller than the previous solution for $\Delta T_{sat} > 100$ K. However, the difference is rather small even at a large ΔT_{sat} (i.e., less than 4% at $\Delta T_{sat} = 350$ K). This indicates that the effect of base flow on δ_{cr} is small. Fig. 5 shows a close up of the solutions of δ_{cr0} corresponding to Fig. 4. Comparison of the present results for $\phi = 0$ reveals that the curves for $\Delta T_{sub} = 5$ K, 30 K, 58 K and 72 K agree almost completely. For $\phi = \pi/2$ rad, on the other hand, δ_{cr} is larger for larger ΔT_{sub}. However, the difference between the cases of $\phi = 0$ and $\phi = \pi/2$ rad is less than $\pm 0.24\%$.

Figs. 6–9, respectively, show the comparison of δ_{cr0} for $\phi = 0$ with the average vapor film thickness at the MHF-point δ_{MHF} for the experimental data by Nishio–Uemura. [8], Dhir–Purohit [19], Kikuchi et al. [20] for the clean sphere, and Kikuchi et al. [20] for the paint-coated sphere. In these figures δ_{cr0} and δ_{MHF} are plotted as a function of ΔT_{sat} with ΔT_{sub} as a parameter. The average vapor film thickness δ obtained from the expression for α_v proposed by Kikuchi et al. [20] is also shown for parametric values of ΔT_{sub}. Since the effect of radiation is neglected in the theoretical model of Kikuchi et al. [20], the value of δ taking account of the radiation effect was estimated by the following equation:

$$\delta = \frac{\lambda_v}{\alpha_v}\left(1 + 0.12\frac{\alpha_r}{\alpha_v}\right) \quad (48)$$

Eq. (48) is derived from the following relation between the heat transfer coefficient for film boiling taking account of the radiation effect and the average vapor film thickness:

$$\alpha_v + 0.88\alpha_r = \frac{\lambda_v}{\delta} + \alpha_r \quad (49)$$

According to the numerical results, the second term on the right hand side of Eq. (48) is negligible as compared to the first term.

Fig. 6 shows the case of 10-mm-dia. sphere by Nishio–Uemura [8]. The δ_{MHF} are plotted using four different symbols depending on the range of ΔT_{sub}. For each range of ΔT_{sub}, δ_{MHF} agrees moderately with δ. The δ_{MHF} decreases with increasing ΔT_{sub} and agrees well with δ_{cr0} for $\Delta T_{sub} = 70$–73 K. It is also seen from Fig. 6 that $\Delta T_{sat,MHF}$ (i.e., value of ΔT_{sat} corresponding to δ_{MHF}) for each range of ΔT_{sub} is scattered within a range and it increases with increasing ΔT_{sub}. The slope of δ is larger

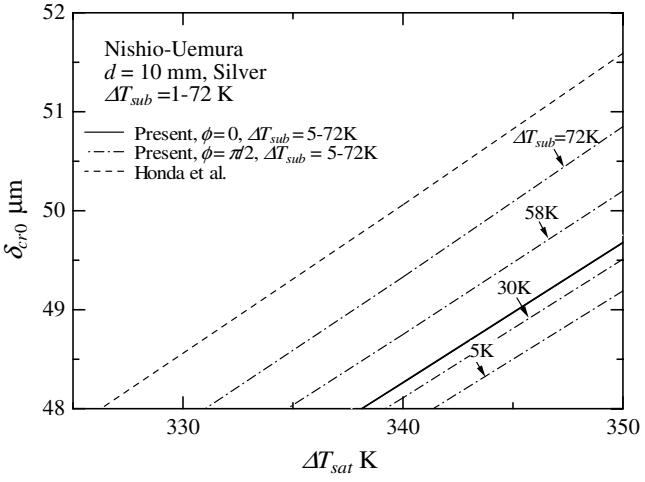

Fig. 5. Variation of δ_{cr0} with ΔT_{sat}.

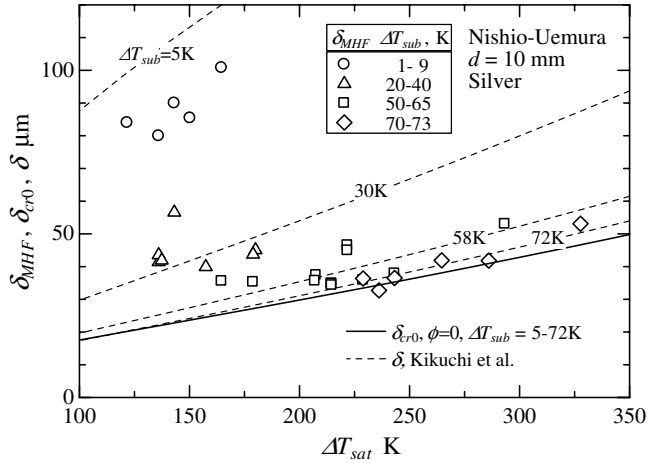

Fig. 6. Variation of δ_{MHF}, δ_{cr0} and δ with ΔT_{sat}: Comparison for Nishio–Uemura data.

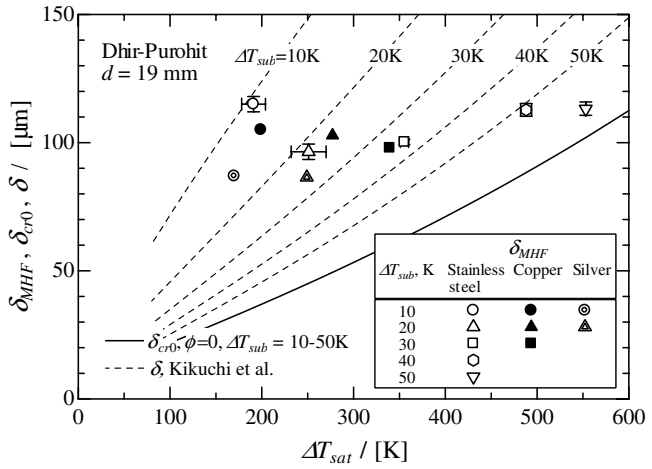

Fig. 7. Variation of δ_{MHF}, δ_{cr0} and δ with ΔT_{sat}: Comparison for Dhir–Purohit data.

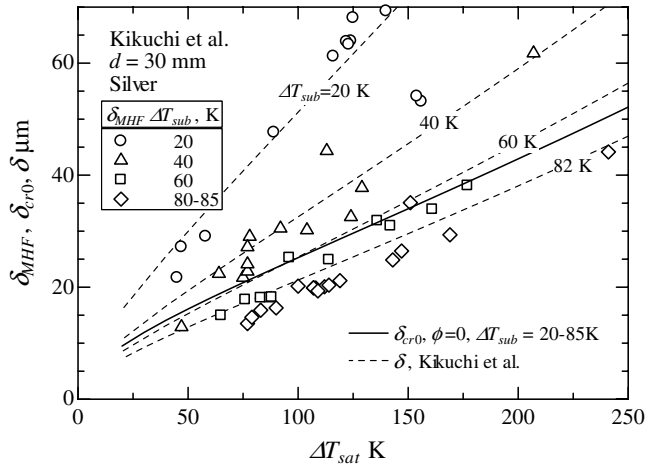

Fig. 8. Variation of δ_{MHF}, δ_{cr0} and δ with ΔT_{sat}: Comparison for Kikuchi et al. data for clean sphere.

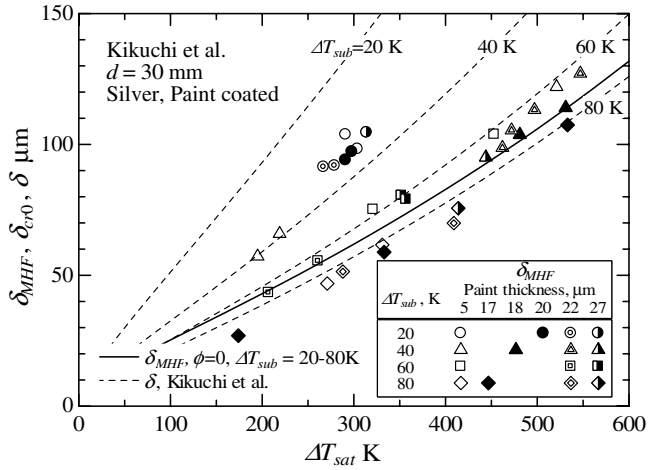

Fig. 9. Variation of δ_{MHF}, δ_{cr0} and δ with ΔT_{sat}: Comparison for Kikuci et al. data for paint coated sphere.

than that of δ_{cr0} and the two curves cross at one point. Theoretically, this indicates that the vapor film is stable for the range of ΔT_{sat} greater than the cross-point and vice versa. Actually, at a low ΔT_{sub}, a part of generated vapor forms vapor bubbles at the top of the sphere and detaches. This will cause a disturbance in the surrounding liquid and vapor film, resulting in the onset of liquid–solid contact and a premature collapse of vapor film. The disturbance will decrease as ΔT_{sub} increases and there will be no vapor bubble formation at a high ΔT_{sub}. This will be the reason for a good agreement between δ_{MHF} and δ_{cr} at $\Delta T_{sub} = 70$–73 K. Even in this case $\Delta T_{sat,MHF}$ is scattered in a range, because the stability of vapor film is very sensitive to a low level of disturbance.

Fig. 7 shows the case of 19-mm-dia. spheres by Dhir–Purohit [19]. While the experimental data show basically the same trend as the case of Nishio–Uemura [8], δ_{MHF} is always greater than δ_{cr0}. The difference between δ_{MHF} and δ_{cr0} decreases as ΔT_{sub} increases. It is also seen from Fig. 7 that for each ΔT_{sub}, δ_{MHF} is consistently smaller than δ.

Fig. 8 shows the case of 30-mm-dia. clean sphere by Kikuchi et al. [20]. The trend of experimental data is basically the same as the cases of Figs. 6 and 7. In Fig. 8, however, δ_{MHF} for $\Delta T_{sub} = 80$–85 K is considerably smaller than δ_{cr0}. This may be ascribed to the fact that the upper part of the test piece was cylindrical in shape. During the experiments, the test piece was immersed in subcooled water up to the middle of the cylindrical part. Thus it is probable that the average vapor film thickness was smaller than that for a sphere. It is also seen from Fig. 8 that the value of δ for $\Delta T_{sub} = 82$ K is also smaller than δ_{cr0} and agrees fairly well with δ_{MHF}. In the absence of detailed information about the theoretical analysis by Kikuchi et al. [20], it is impossible to discuss the reason for this result.

Fig. 9 shows the case of 30-mm-dia. paint-coated sphere by Kikuchi et al. [20]. The range of $\Delta T_{sat,MHF}$ is much higher than that of clean sphere shown in Fig. 8. However, the trend of experimental data is basically the same as the case of clean sphere. The difference between δ_{MHF} and δ_{cr0} at $\Delta T_{sub} = 80$ K is smaller than that for the clean sphere and a fairly good agreement between the two is obtained at a high ΔT_{sat}.

It is relevant to discuss here the effects of k and s on the mode of vapor film collapse. The present analysis shows that the vapor film is most unstable for $k = 0$ (i.e., uniform disturbance). This will be the main reason for an instantaneous collapse of vapor film observed in the experiments. In Fig. 3a, the value of amplification factor s_r corresponding to the case of $k = 0$ is about $35\ s^{-1}$ and $168\ s^{-1}$ for $\delta_0 = 0.99\delta_{cr0}$ and $\delta_0 = 0.95\delta_{cr0}$, respectively. For the experimental data cited in Figs. 6–9, the calculated value of frequency s_i corresponding to δ_{cr0} ranges from 2.9 kHz to 8.1 kHz. Thus the amplification factor and frequency of disturbance are high enough to cause an instantaneous collapse of vapor film.

According to the temperature-controlled hypothesis of the MHF-point condition [6–8], liquid–solid contact occurs only when the wall temperature is below the thermodynamic superheat limit of liquid. The wall superheat at the instant of liquid–solid contact at the MHF-point $\Delta\widetilde{T}_{\mathrm{sat,MHF}}$ is given by the solution of unsteady heat conduction as follows:

$$\Delta\widetilde{T}_{\mathrm{sat,MHF}} = \frac{(\lambda_{\mathrm{w}}\rho_{\mathrm{w}}C_{\mathrm{w}})^{1/2}\Delta T_{\mathrm{sat,MHF}}}{(\lambda_{\mathrm{w}}\rho_{\mathrm{w}}C_{\mathrm{w}})^{1/2} + (\lambda_{\mathrm{l}}\rho_{\mathrm{l}}C_{\mathrm{l}})^{1/2}} \tag{50}$$

where C_{w} and C_{l} denote the specific heats of wall and liquid, respectively. Table 2 summarizes the values of $\Delta T_{\mathrm{sat,MHF}}$ and $\Delta\widetilde{T}_{\mathrm{sat,MHF}}$ for the experiments conducted by Nishio–Uemura [8], Dhir–Purohit [19] and Kikuchi et al. [20]. For the paint coated sphere by Kikuchi et al. [20], the physical properties of sphere surface were approximated by those of silicone resin. The difference between $\Delta T_{\mathrm{sat,MHF}}$ and $\Delta\widetilde{T}_{\mathrm{sat,MHF}}$ is largest for the paint coated sphere with the smallest value of $\lambda_{\mathrm{w}}\rho_{\mathrm{w}}C_{\mathrm{w}}$. Comparison of the maximum value of $\Delta\widetilde{T}_{\mathrm{sat,MHF}}$ with the limiting liquid superheat of water predicted by the Lienhard equation [22] (=217.3 K) reveals that the former is larger than the latter by 233.6 K, 93.7 K and 11.9 K for the clean sphere data by Dhir–Purohit [19], Nishio–Uemura [8] and Kikuchi et al. [20], respectively. For the paint coated sphere by Kikuchi et al. [20], on the other hand, the maximum value of $\Delta\widetilde{T}_{\mathrm{sat,MHF}}$ is smaller than the limiting liquid superheat by 58.8 K. It should be mentioned here that the values of $\Delta\widetilde{T}_{\mathrm{sat,MHF}}$ for the clean sphere by Kikuchi et al. [20] are smaller than the limiting liquid superheat except for one data mentioned above. Thus it may be concluded that the temperature-controlled hypothesis of the MHF-point condition is supported by the clean sphere and paint coated sphere data by Kikuchi et al. [20]. This hypothesis is not supported by the clean sphere data by Dhir–Purohit [19] and Nishio–Uemura[8].

The maximum value of $\Delta\widetilde{T}_{\mathrm{sat,MHF}}$ for each experiment is connected with the trend of $\Delta T_{\mathrm{sat,MHF}}$ versus ΔT_{sub} relation shown in Fig. 2. For the experimental data by Dhir–Purohit [19] and Nishio–Uemura [8], $\Delta T_{\mathrm{sat,MHF}}$ increases with increasing ΔT_{sub}. The increase is more significant for the Dhir–Purohit [19] data with a larger maximum value of $\Delta\widetilde{T}_{\mathrm{sat,MHF}}$. For the experimental data by Kikuchi et al. [20], on the other hand, $\Delta T_{\mathrm{sat,MHF}}$ shows no dependence on ΔT_{sub}. The test sphere of Dhir–Purohit [19] was supported on a vertical stem of relatively small diameter (=3 mm). Thus it is probable that the local wall temperature at the connecting point between the test sphere and the stem was much lower than the average wall temperature. This indicates that the experimental data were affected by the propagative collapse of vapor film which started at the connecting point. The experimental data by Nishio–Uemura [8] are supposed to be slightly affected by the propagative collapse. For the experiments by Kikuchi et al. [20], non-uniformity of wall temperature is supposed to be much smaller than the cases of Dhir–Purohit [19] and Nishio–Uemura [8], because the test piece was immersed in subcooled water up to the middle of the cylindrical part with a relatively large diameter (=8 mm). Thus their experimental data are supposed to be not affected by the propagative collapse. More experiments are needed to clarify this point.

3. Concluding remarks

A linear stability analysis of vapor film in subcooled film boiling on a sphere taking account of interaction between main flow and perturbed components was presented. A small disturbance of standing wave type was assumed to be superimposed on the base flows of surrounding liquid and vapor film. By using compatibility conditions at the liquid–vapor interface, the solutions for the surrounding liquid and vapor film were combined to yield an algebraic relation among the vapor film thickness, the order of disturbance and the complex amplification factor of disturbance. For given conditions of the sphere and surrounding liquid, the critical vapor film thickness δ_{cr} below which the vapor film is unstable was obtained for the disturbances of the orders of 0, 1 and 2. The effects of base flow and liquid subcooling ΔT_{sub} on the value of δ_{cr} was small. The δ_{cr} was largest for the disturbance of the zeroth order (i.e., uniform disturbance). This indicated that the stability limit of subcooled film boiling was determined by the value of δ_{cr} for the uniform disturbance, δ_{cr0}.

The calculated values of δ_{cr0} were compared with the average vapor film thicknesses at the MHF-point δ_{MHF} obtained from the immersion cooling experiments of spheres in subcooled water conducted by Nishio–Uemura [8], Dhir–Purohit [19] and Kikuchi et al. [20]. At a low ΔT_{sub}, δ_{MHF} was much larger than δ_{cr0}. The δ_{MHF} decreased with increasing ΔT_{sub} and compared well with δ_{cr0} for $\Delta T_{\mathrm{sub}} > 60$K. Thus it may be concluded that the stability limit of vapor film described in the present paper is an

Table 2
Values of $\Delta T_{\mathrm{sat,MHF}}$ and $\Delta\widetilde{T}_{\mathrm{sat,MHF}}$ for each experimental condition

Author	Material	Surface condition	$\Delta T_{\mathrm{sat,MHF}}$, K	$\Delta\widetilde{T}_{\mathrm{sat,MHF}}$, K
Nishio–Uemura	Silver	Clean	121.7–327.7	115.7–311.0
Dhir–Purohit	Stainless steel	Clean	178–533	150.6–450.9
	Copper	Clean	190–352	182.0–337.2
	Silver	Clean	165–270	156.9–256.8
Kikuchi et al.	Silver	Clean	45–241	42.8–229.2
		Paint coated	174–547	50.4–158.5

important element of the MHF-point condition of highly subcooled film boiling.

Comparison of the wall superheat at the instant of liquid–solid contact at the MHF-point $\Delta\widetilde{T}_{\mathrm{sat,MHF}}$ with the limiting superheat of water revealed that the maximum value of $\Delta\widetilde{T}_{\mathrm{sat,MHF}}$ was comparable to or smaller than the limiting liquid superheat for the experimental data that was supposed to be not affected by the propagative collapse of vapor film. The maximum value of $\Delta\widetilde{T}_{\mathrm{sat,MHF}}$ was larger than the limiting liquid superheat for the experimental data that was supposed to be affected by the propagative collapse of vapor film.

Appendix A

The average heat flux used for evaporation at the liquid–vapor interface q_{ev0} is related to the flow rate of vapor leaving the sphere M_{v} by the following equation:

$$h_{\mathrm{lg}}M_{\mathrm{v}} = \pi d^2 q_{\mathrm{ev0}} \tag{A1}$$

The M_{v} can be expressed in terms of the circumferential vapor velocity at $\phi = \pi/2$ as follows:

$$M_{\mathrm{v}} = a\pi d\rho_{\mathrm{v}} \int_0^{\delta_0} u_{\mathrm{v0}}\,\mathrm{d}y = \frac{a\pi d\rho_{\mathrm{v}}(\rho_{\mathrm{l}}-\rho_{\mathrm{v}})g\delta_0^3}{12\mu_{\mathrm{v}}} \tag{A2}$$

where a is the proportionality constant and δ_0 is the vapor film thickness at $\phi = \pi/2$.

For saturated boiling, all the heat transferred is used for evaporation. Thus q_{ev0} can be expressed as follows:

$$q_{\mathrm{ev0}} = (\alpha_{\mathrm{vs}} + 0.88\alpha_{\mathrm{r}})\Delta T_{\mathrm{sat}} \tag{A3}$$

Also, δ_0 may be approximated by the following equation:

$$\delta_0 = \lambda_{\mathrm{v}}/\alpha_{\mathrm{vs}} \tag{A4}$$

Elimination of M_v, q_{ev0} and δ_0 from Eqs. (A1)–(A4) yields the following solution for a:

$$a = \frac{12\mu_{\mathrm{v}}d(\alpha_{\mathrm{vs}}+0.88\alpha_{\mathrm{r}})}{h_{\mathrm{lg}}\rho_{\mathrm{v}}(\rho_{\mathrm{l}}-\rho_{\mathrm{v}})g}\left(\frac{\alpha_{\mathrm{vs}}}{\lambda_{\mathrm{v}}}\right)^3\Delta T_{\mathrm{sat}} \tag{A5}$$

Substitution of Eq. (A5) into Eq. (A2), and then substitution of M_v given by the resulting equation into Eq. (A1) yields the following general expression for q_{ev0}:

$$q_{\mathrm{ev0}} = (\alpha_{\mathrm{vs}} + 0.88\alpha_{\mathrm{r}})\left(\frac{\alpha_{\mathrm{vs}}\delta_0}{\lambda_{\mathrm{v}}}\right)^3\Delta T_{\mathrm{sat}}. \tag{A6}$$

References

[1] S. Nishio, Prediction technique for minimum-heat-flux(MHF)-point condition of saturated film boiling, Int. J. Heat Mass Transfer 30 (10) (1987) 2045–2057.

[2] W.S. Bradfield, Liquid–solid contact in stable film boiling, I & EC Fundamentals 5 (2) (1966) 200–204.

[3] S.C. Yao, R.E. Henry, An investigation of the minimum film boiling temperature on horizontal surfaces, ASME J. Heat Transfer 100 (2) (1978) 260–267.

[4] D.S. Dugha, R.H.S. Winterton, Measurement of surface contact in transition boiling, Int. J. Heat Mass Transfer 18 (10) (1985) 1869–1880.

[5] M. Shoji, L.C. Witte, S. Yokoya, M. Ohshima, Liquid–solid contact and effects of surface roughness and wettability in film and transition boiling on a horizontal large surface, in: Proc. 9th Int. Heat Transfer Conf., Jerusalem, Israel, Hemisphere 2 (1990) 135–140.

[6] P. Spiegler, P.J. Hopenfeld, M. Silberberg, C.F. Bumpus Jr., A. Norman, Onset of stable film boiling and the foam limit, Int. J. Heat Mass Transfer 6 (11) (1963) 987–989.

[7] A. Segev, S.G. Bankoff, The role of adsorption in determining the minimum film boiling temperature, Int. J. Heat Mass Transfer 23 (5) (1980) 637–642.

[8] S. Nishio, M. Uemura, Study on film boiling heat transfer and minimum heat flux condition for subcooled boiling (1st Report, pool boiling of water at atmospheric pressure from platinum sphere), Trans. JSME, Ser. B 52 (476) (1986) 1811–1816.

[9] N. Zuber, Hydrodynamic aspects of boiling heat transfer, Atomic Energy Commision Report No. AECU-4439, Univ. California, Los Angels, Physics and Mathematics, 1959.

[10] J.H. Lienhard, P.T.Y. Wong, The dominant unstable wavelength and minimum heat flux during film boiling on a horizontal cylinder, Trans. ASME J. Heat Transfer 86 (1) (1964) 220–226.

[11] J.H. Lienhard, V.K. Dhir, On the prediction of the minimum pool boiling heat flux, Trans. ASME J. Heat Transfer 102 (3) (1980) 457–460.

[12] F.S. Gunnerson, A.W. Cronenberg, On the minimum film boiling conditions for spherical geometries, Trans. ASME J. Heat Transfer 102 (2) (1980) 335–341.

[13] J.M. Ramillison, J.H. Lienhard, Transition boiling heat transfer and the film transition regime, Trans. ASME J. Heat Transfer 109 (3) (1987) 746–752.

[14] G.I. Taylor, The instability of liquid surfaces when accelerated in a direction perpendicular to their planes, I, Proc. Roy. Soc. London, Ser. A 201 (1950) 192–196.

[15] H. Honda, H. Takamatsu, H. Yamashiro, Heat transfer characteristics during rapid quenching of a thin wire in water, Heat Transfer Jpn. Res. 21 (8) (1992) 773–791.

[16] H. Honda, H. Takamatsu, H. Yamashiro, Heat transfer and liquid–solid contact during rapid quenching of a thin wire in water and $CaCl_2$/water solution, in: Proc. 10th Int. Heat Transfer Conf., Brighton, UK, Inst. Chem. Engrs 5 (1994) 57–62.

[17] H. Honda, H. Yamashiro, H. Takamatsu, Effect of the behavior of generated vapor on the minimum-heat-flux point during rapid quenching of a thin horizontal wires, in: Proc. 5th ASME/JSME Joint Thermal Engineering Conf., San Diego, USA, ASME, Paper AJTE99-6366, 1999.

[18] H. Honda, H. Yamashiro, H. Takamatsu, Stability of vapor film in subcooled film boiling on a sphere, Therm. Sci. Eng. 7 (5) (1999) 1–10.

[19] V.K. Dhir, G.P. Purohit, Subcooled film-boiling heat transfer from sphere, Nucl. Eng. Des. 47 (1) (1978) 49–66.

[20] Y. Kikuchi, M. Nagase, I. Michiyoshi, On the low limit of subcooled film boiling, Trans. JSME B 506 (54) (1988) 2830–2837.

[21] J.C.Y. Koh, Analysis of film boiling on vertical surfaces, Trans. ASME J. Heat Transfer 84 (1) (1962) 55.

[22] J.H. Lienhard, Corresponding state correlation for spinodal and homogeneous nucleation temperature, Trans. ASME J. Heat Transfer 104 (2) (1982) 379–381.